Variability of Warm Deep Water Inflow in a Submarine Trough on the Amundsen Sea Shelf

A. K. WÅHLIN, O. KALÉN, L. ARNEBORG, AND G. BJÖRK

Department of Earth Sciences, University of Gothenburg, Gothenburg, Sweden

G. K. CARVAJAL

Chalmers University of Technology, Gothenburg, Sweden

H. K. HA, T. W. KIM, AND S. H. LEE

Division of Polar Climate Research, Korea Polar Research Institute, Incheon, South Korea

J. H. LEE

Ocean Circulation and Climate Research Division, Korea Institute of Ocean Science and Technology, Ansan, South Korea

C. STRANNE

Department of Earth Sciences, University of Gothenburg, Gothenburg, Sweden

(Manuscript received 23 August 2012, in final form 2 April 2013)

ABSTRACT

The ice shelves in the Amundsen Sea are thinning rapidly, and the main reason for their decline appears to be warm ocean currents circulating below the ice shelves and melting these from below. Ocean currents transport warm dense water onto the shelf, channeled by bathymetric troughs leading to the deep inner basins. A hydrographic mooring equipped with an upward-looking ADCP has been placed in one of these troughs on the central Amundsen shelf. The two years (2010/11) of mooring data are here used to characterize the inflow of warm deep water to the deep shelf basins. During both years, the warm layer thickness and temperature peaked in austral fall. The along-trough velocity is dominated by strong fluctuations that do not vary in the vertical. These fluctuations are correlated with the local wind, with eastward wind over the shelf and shelf break giving flow toward the ice shelves. In addition, there is a persistent flow of dense lower Circumpolar Deep Water (CDW) toward the ice shelves in the bottom layer. This bottom-intensified flow appears to be driven by buoyancy forces rather than the shelfbreak wind. The years of 2010 and 2011 were characterized by a comparatively stationary Amundsen Sea low, and hence there were no strong eastward winds during winter that could drive an upwelling of warm water along the shelf break. Regardless of this, there was a persistent flow of lower CDW in the bottom layer during the two years. The average heat transport toward the ice shelves in the trough was estimated from the mooring data to be 0.95 TW.

1. Introduction

The ice shelves in the Amundsen Sea that drain the West Antarctic Ice Sheet are thinning rapidly (e.g., Shepherd et al. 2001, 2004; Pritchard et al. 2009, 2012). The main reason for their decline appears to be warm ocean currents circulating below the ice shelves and melting the glacial ice from below (Jacobs et al. 2011; Pritchard et al. 2012). Ocean currents transport warm dense water onto the shelf, channeled by bathymetric troughs leading to the deep inner basins, for example, in the Marguerite Trough (Klinck et al. 2004; Moffat et al. 2009; Dinniman et al. 2011) and on the Amundsen shelf (Walker et al. 2007; Wåhlin et al. 2010; Jacobs et al. 2011). Despite the global importance of this part of the climate system, the Amundsen and Bellingshausen Seas

Corresponding author address: A. K. Wåhlin, Department of Earth Sciences, University of Gothenburg, Box 460, 405 30 Gothenburg, Sweden.
E-mail: awahlin@gu.se

DOI: 10.1175/JPO-D-12-0157.1

remain relatively poorly sampled and several aspects of their general physical oceanography are still unknown.

Deep water as warm as 3°C above freezing has been observed on the whole Amundsen shelf and as far west as the western terminus of Getz ice shelf (Jacobs et al. 2012). The warm water on the shelf is colder, fresher, and less dense the farther west it resides (Jacobs et al. 2012; Yuan et al. 2013, manuscript submitted to *J. Geophys. Res.*). A significant interannual variability in temperature, salinity, and warm layer thickness is evident (Jacobs et al. 2012), making it difficult to identify trends in the hydrography. Because of the scarcity of observations in the region, the physical mechanisms behind the forcing of the warm deep water onto the shelf are still basically unknown. It is also not known how the dense water circulates on the shelf, although recent observations (H. K. Ha et al. 2013, unpublished manuscript) and model studies (Schodlok et al. 2012; St. Laurent et al. 2013) indicate that horizontal circulation cells on the shelf may be of importance. To address these questions, longer time series of measurements of the warm deep currents are necessary. Model studies from the Amundsen Sea suggest that eastward winds force flow of warm deep water onto the shelf (Thoma et al. 2008, hereafter T08; Steig et al. 2012, hereafter S12). Eastward winds at the shelf break are associated with northward Ekman transport in the surface layer, and a compensating southward return flow below the surface. The models show a seasonal variation with maximum warm layer thickness during September–November, attributed to the seasonality of the wind field (T08; S12). A more recent model study with higher-resolution bathymetry (Schodlok et al. 2012) forced by an improved wind reanalysis product (Dee et al. 2011) shows instead a seasonal variation with maximum heat transport toward the ice shelf cavities in March–May. Neither of these models, however, has been validated with time series data from the Amundsen Sea.

To understand the across-shelf forcing of the warm water flow on the central Amundsen shelf, a mooring recording velocity, temperature, and salinity was placed on the eastern side of the submarine trough leading to the deep shelf basins. Analysis of the first year observations (Arneborg et al. 2012) showed that warm water was present throughout the year at the bottom of the trough with an average transport of warm water toward the ice shelves. Superposed on this was a fluctuating barotropic flow that did not contribute to the long-term heat transport. In the present study the measurement period is extended to over two full years, permitting a first assessment of seasonal dependence and a quantitative analysis of the wind effects. Historical and newly acquired CTD data are furthermore used to address the question of the origin of the warm water found on the central shelf.

2. Methods

The data presented here were obtained from a mooring placed at 72.46°S, 116.35°W, in one of the deep troughs that crosses the central Amundsen shelf (Fig. 1). It was deployed on 15 February 2010, recovered and redeployed on 25 December 2010, and recovered again on 1 March 2012. The mooring consisted of 5 (7 during the second deployment period in 2011) Sea-Bird Electronics (SBE) 37 Serial interface, memory, integral pump, and integrated dissolved oxygen (SMP) CTD recorders with an accuracy of 0.003 K for the deployment period, evenly spaced between the bottom at 540- and the top buoy at 320-m depth, and an upward-looking 150-kHz RD Instruments (RDI) Workhorse Acoustic Doppler Current Profiler (ADCP) at the bottom. The ADCP was configured in narrowband mode for optimal range, using 8-m bins and 15-min ensembles of 25 pings each. The data were processed using the WinADCP software, filtering out data with error velocity exceeding $1.5\,\mathrm{cm\,s^{-1}}$ and beam correlation below 100. Daily averages of detided velocity [using the t_tide harmonic analysis per Pawlowicz et al. (2002)] were decomposed into its empirical orthogonal function (EOF; e.g., Davis 1976) modes. Because of large error velocity and/or low beam correlation, the data above 340- (360) m depth in 2010 (2011), respectively, were removed. The EOF modes were calculated for the two years of data separately, in which case data from the bottom up to 340 (360)-m depth were used for 2010 (2011), and also as one single time series for 2010/11, in which case only data from the bottom up to 360-m depth were used. In addition to the mooring data, CTD data obtained during cruises with IB *Oden* in 2008/09 and 2010/11 and IB *Araon* in 2010/11 and early 2012 were used. In these cruises, profiles for temperature (with an accuracy of 0.001 K), conductivity (with an accuracy of $0.0003\,\mathrm{S\,m^{-1}}$), and depth were collected with a Sea-Bird 911 plus system. The sensors were calibrated before and after the cruises and corrected for any drift.

Because of the velocity of the water, heat energy is transported past the mooring. A heat flux vector $\mathbf{q}_H$ ($\mathrm{J\,m^{-2}\,s^{-1}}$) can be calculated according to

$$\mathbf{q}_H = \rho C_P \mathbf{U}(T - T_R), \tag{1}$$

where ρ ($\mathrm{kg\,m^{-3}}$) is the density, C_P ($\mathrm{J\,K^{-1}\,kg^{-1}}$) is the specific heat capacity, $\mathbf{U}$ ($\mathrm{m\,s^{-1}}$) is the velocity vector, T (K) is the temperature, and T_R (K) is a reference temperature. The total heat transport Q_H ($\mathrm{J\,s^{-1}}$) through

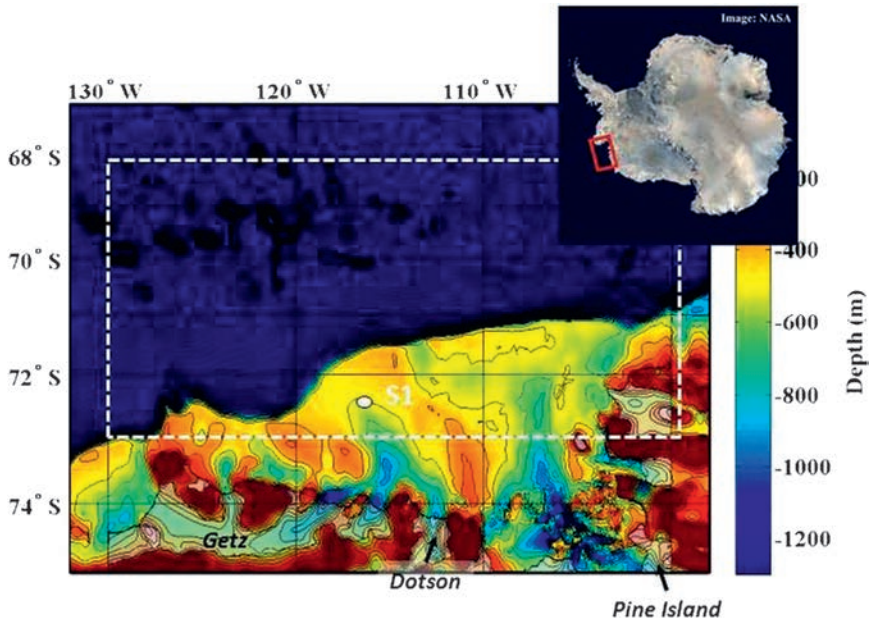

FIG. 1. Map of the region with the position of the mooring S1 indicated by white ellipse. The white dashed rectangle shows the region over which the wind field is averaged in Figs. 2 and 9.

the channel is obtained by integrating Eq. (1) vertically and across the trough

$$Q_H = \iint \rho C_P U_P (T - T_R)\, dz\, dx, \qquad (2)$$

where U_P ($\mathrm{m\,s^{-1}}$) is the along-channel velocity component, z is the vertical coordinate, and x is the across-trough coordinate. For the mooring heat flux calculations an effective width of 80 km is assumed, based on the cross-trough CTD sections in Wåhlin et al. (2010) and Arneborg et al. (2012) that show the approximate slope of the isotherms.

Comparisons between the mooring data and the wind are obtained by using European Centre for Medium-Range Weather Forecasts (ECMWF) Interim Re-Analysis (ERA-Interim) wind data (Dee et al. 2011), which according to Bracegirdle and Marshall (2012) is the most accurate of the six major meteorological reanalysis products covering the Amundsen Sea. Bracegirdle and Marshall (2012) found generally good agreement between the ERA-Interim and independent data in the Bellingshausen Sea. Figure 2 shows a comparison between the ERA-Interim and in situ wind data from Lindsey Island (Lee et al. 2012). The correlation between the two datasets is 0.89. The average eastward velocity is $-6.4\,\mathrm{m\,s^{-1}}$ for Lindsey Island, compared to the ERA-Interim, which is $-3.3\,\mathrm{m\,s^{-1}}$. This difference may be due to local wind conditions at Lindsey Island. Also shown are average values produced from a new algorithm processing Advanced Synthetic Aperture Radar (ASAR) data described by Carvajal et al. (2013), which is not hitherto included in the reanalysis. The data obtained from the Carvajal SAR wind algorithm have temporal resolution limited by the passage of *Envisat*, the activity of the ASAR instrument, and the ice coverage. The values shown in Fig. 2 were computed from portions of ASAR images with coverage in the area of study (white rectangle of Fig. 1). Since the ASAR data are restricted to a maximum of three images per day within the area of interest, which are nearly always incomplete, images from a 48-h window were used so that data from up to six ASAR images could be included. Figure 2d shows a gridpoint scatter comparison of the Carvajal algorithm and the reanalysis data, with the Carvajal data points represented by the spatial average of all points lying within the ECMWF grid square, and the ERA-Interim data chosen at the time closest to the *Envisat* passage (at most 3-h difference). In similarity with the Bracegirdle and Marshall (2012) results, the ERA-Interim data compare favorably with the two independent datasets here, in both spatial and temporal variation.

3. Results

Figure 3 shows daily averages of temperature and salinity, interpolated to the ADCP bin depths. As noted in Arneborg et al. (2012) for the 2010 data, there is a continuous presence of warm deep water near the bottom of the trough. The temperature and salinity also

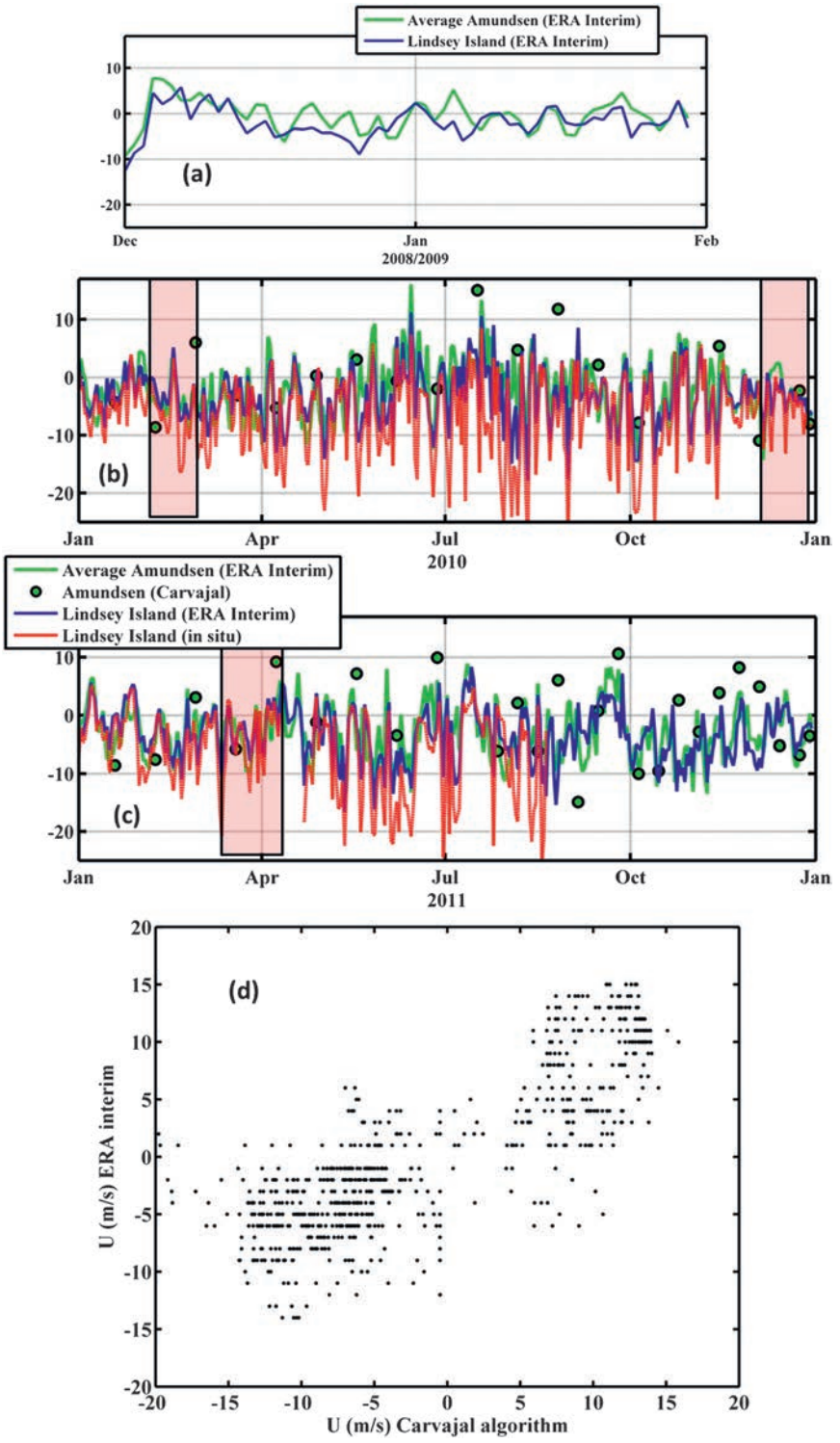

FIG. 2. Daily averages of the ERA-Interim eastward wind component. Blue shows values from 73.5°S, 103°W; green shows average wind over the area marked by the white rectangle in Fig. 1; red shows in situ data from Lindsey Island at 73.6°S, 103°W. Green circles show velocities derived from ASAR images according to the method described in Carvajal et al. (2013): (a) December 2008–January 2009 (only ERA-Interim), (b) 2010, and (c) 2011. The red-shaded regions indicate time periods of strong inflow discussed in section 4. (d) Scatterplot of data from individual grid cells from the Carvajal et al. data and from the ERA-Interim.

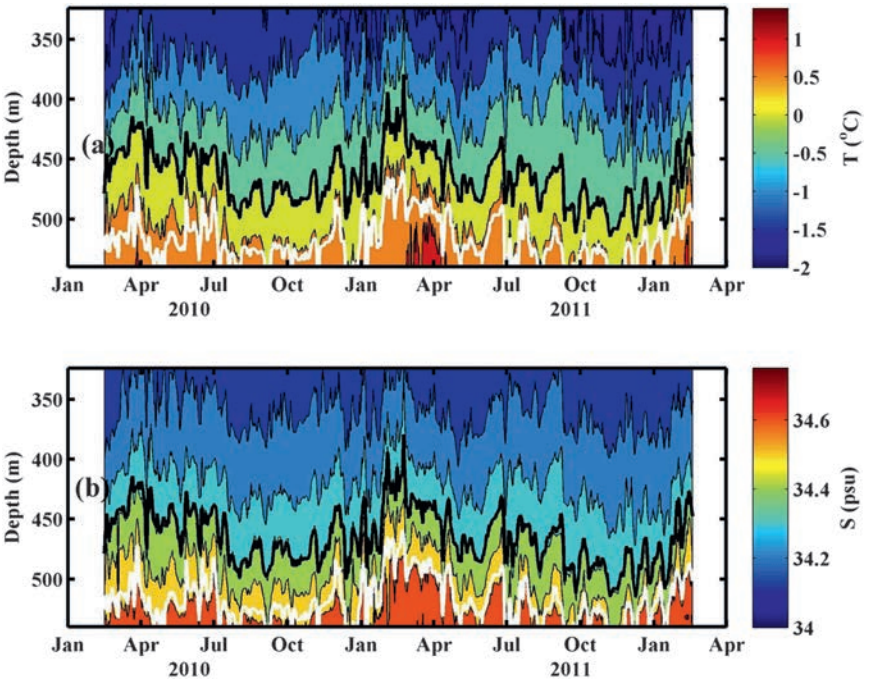

FIG. 3. Daily averages of mooring (a) temperature and (b) salinity as a function of time and depth. The white line shows the isoline for neutral density (Jackett and McDougall 1997) $\gamma_N = 28.03\ \mathrm{kg\,m^{-3}}$. The contour intervals are 0.5°C in (a) and 0.1 psu in (b).

show a pronounced seasonal variation. The maximum thickness of the warm layer, which coincides with the warmest bottom temperature, occurs in March–May. A thinner layer containing cooler and fresher deep water is found in September–November, when the winter mixed layer is also at its deepest and reaches down to about 350 m.

Figure 4a shows a progressive vector plot of the hourly ADCP velocity, color coded by temperature. Also shown is a line indicating the direction of the trough (i.e., 132° compass direction). There is a persistent flow of warm water toward the southeast along the trough near the bottom. Figure 4b shows temporal averages of along- and across-trough velocity components, U and V, respectively. The average velocity in the along-trough direction increases from $1\ \mathrm{cm\,s^{-1}}$ at about 360-m depth to about $4\ \mathrm{cm\,s^{-1}}$ next to the bottom, with the vertical average $2.4\ \mathrm{cm\,s^{-1}}$ (it should be kept in mind that the velocity measurements only cover the lower 240 m, and the currents above this depth are unknown). The cross-trough velocity component has a comparatively small vertical variation and a mean of about $-0.5\ \mathrm{cm\,s^{-1}}$. The marked reduction in velocity in the two lower bins that can be seen in the along-trough velocity is only present in the 2011 data. It could possibly be caused by local topography. Figure 4c shows the temporal average of temperature and salinity, both of which increase approximately linearly with depth. The average temperature increases from −1.5°C at 320-m depth to about 0.8°C near the bottom.

In Fig. 5, daily averages of the along-trough velocity component have been plotted. There is an energetic component of the flow that fluctuates on time scales shorter than monthly. The vertical variation and magnitude of this component can be obtained from EOF analysis. Figure 5b shows the percentage of the total variance that lies in each of the EOF modes. The first mode (EOF1) explains about 90% of the variance, the second (EOF2) explains about 7%, and the third and higher modes give a negligible contribution. Figure 5c shows the amplitude of EOF1 and EOF2 as a function of depth. While EOF1 is nearly depth independent, EOF2 has a vertical structure that changes direction with depth. The first mode (EOF1) has been plotted in Fig. 5d. It dominates the time-varying part of the current velocities and may be interpreted as a barotropic mode modified by bottom friction (remembering that less than half the water column is observed). If this strong fluctuating component is removed from the velocity field, the bottom-intensified residue flow becomes visible. This has been done in Fig. 5e, which shows the difference between the along-trough velocity and EOF1. The residue is dominated by the mean flow toward the coast (Fig. 4b). It also has a fluctuating part, EOF2, which

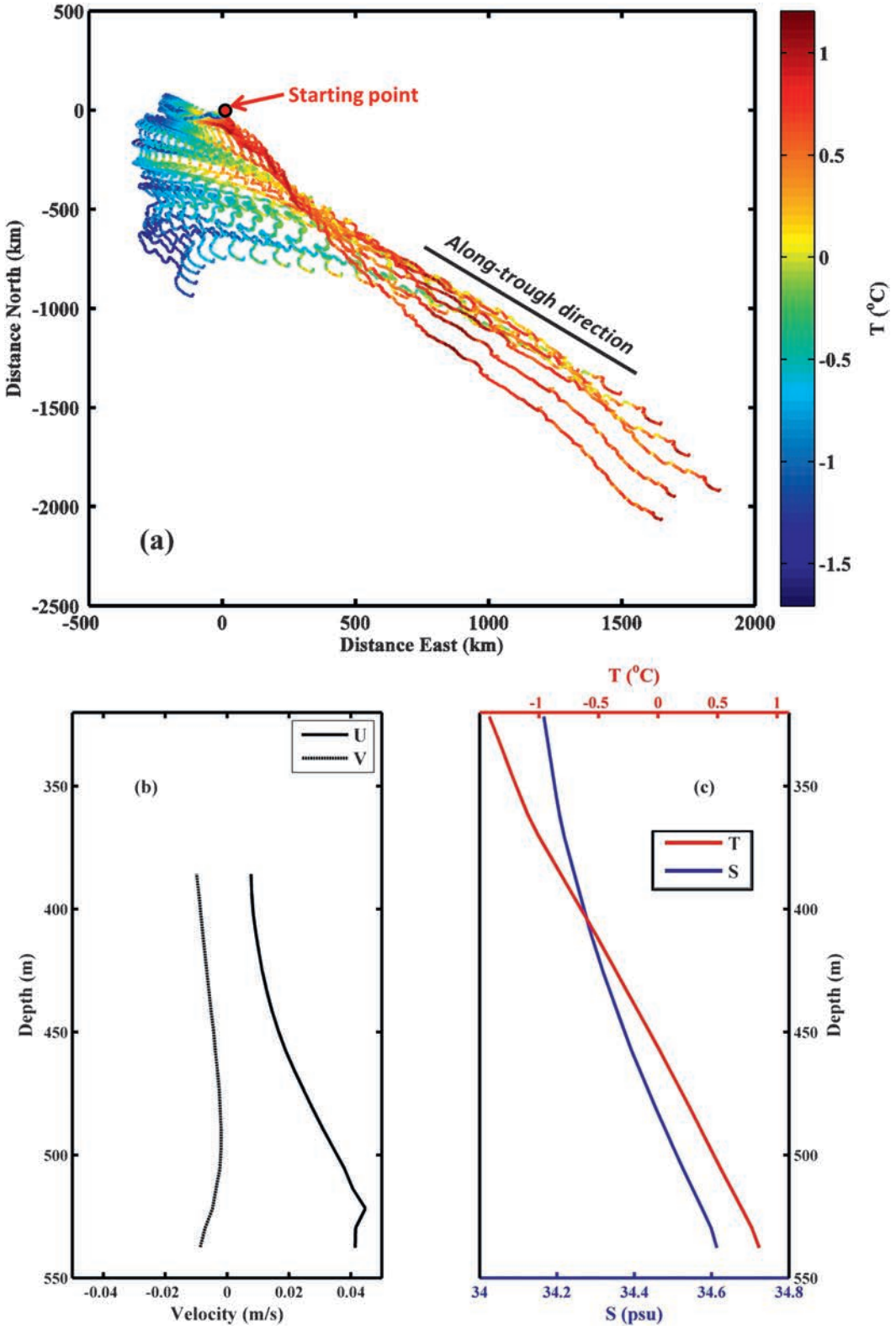

FIG. 4. (a) Progressive vector plot of ADCP velocity, color coded by temperature according to legend. The red circle indicates the starting point for the vectors. (b) Temporal average of along-trough U and across-trough V velocity components according to legend. (c) Temporal average of salinity S and temperature T according to legend.

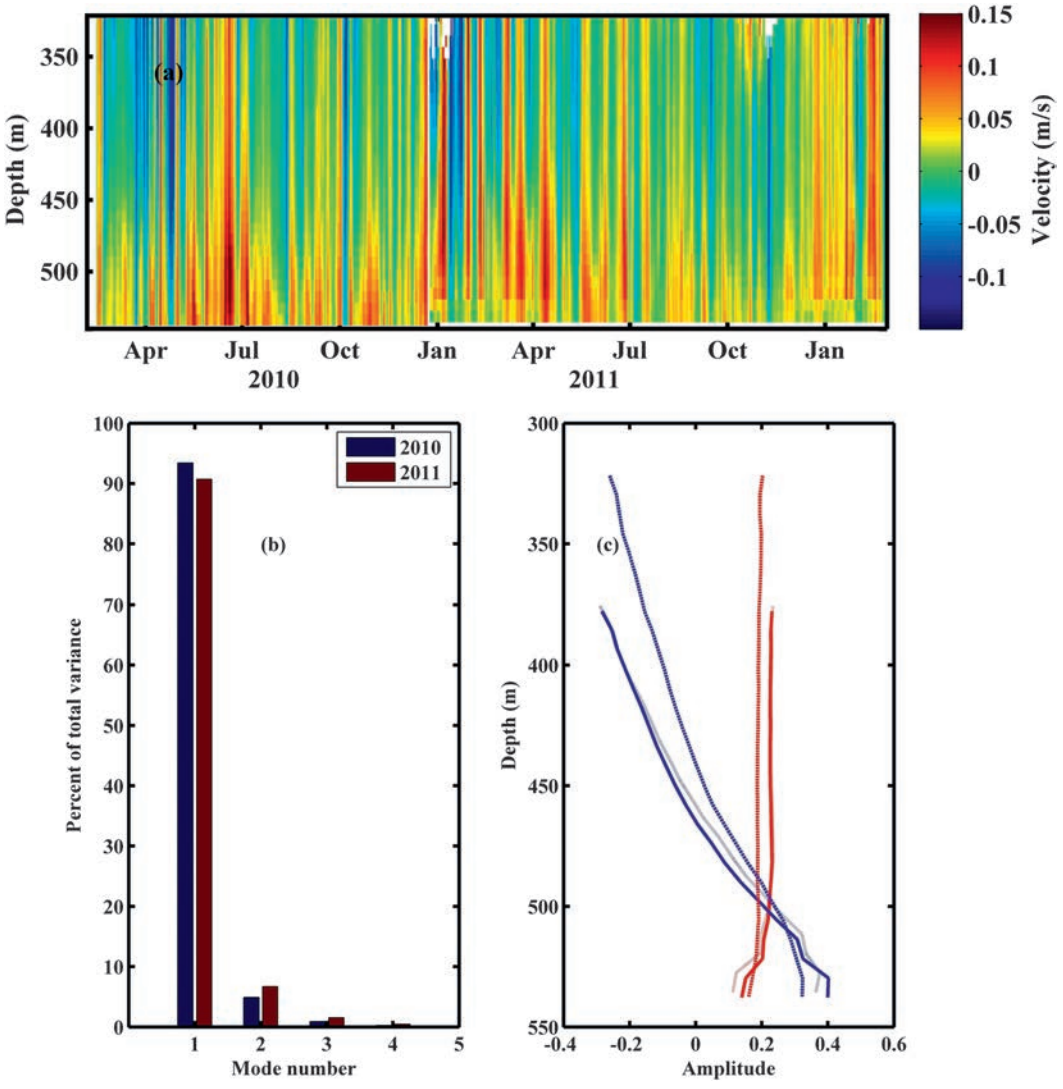

FIG. 5. (a) Daily average of the along-trough velocity (positive values indicating southeastward flow) as a function of time and depth. (b) Percent of total variance that is explained by the first five EOF modes for the two years 2010 and 2011. (c) Shape of the first (red) and second (blue) EOF modes as a function of depth for 2010 (dashed), 2011 (dotted), and for the whole measurement period (solid). (d) The first EOF mode for the whole measurement period. (e) Along-trough residue current, that is, velocity minus the first EOF mode, with positive values indicating southward flow. Black line is the 0°C isotherm.

strengthens and weakens the bottom-intensified mean flow. The results of the EOF analysis will be used for examining the correlation between along-trough velocity and other parameters, such as the wind and the bottom temperature. According to Fig. 5b, 97% of the variance is contained in the two time series EOF1 and EOF2. This is sufficient for our purposes and greatly simplifies the analyses. Since the vertical structure is so different between EOF1 and EOF2, it is expected that the two modes may correlate to different forcing mechanisms. For example, EOF1 may be coupled to a physical forcing giving a barotropic response in the water column and EOF2 to processes giving a baroclinic response.

In Fig. 6, daily and monthly averages of EOF1 and EOF2 are plotted together with bottom temperature and salinity. In similarity with temperature and salinity, EOF2 also has high values in March–May, and the temperature and salinity covary to some extent with EOF2. A similar behavior can be seen in Fig. 5e where the 0°C isotherm, indicative of the warm-layer thickness, follows the thickness of the residue inflow. This is confirmed by the correlation between the EOF modes and bottom temperature. The maximum correlation

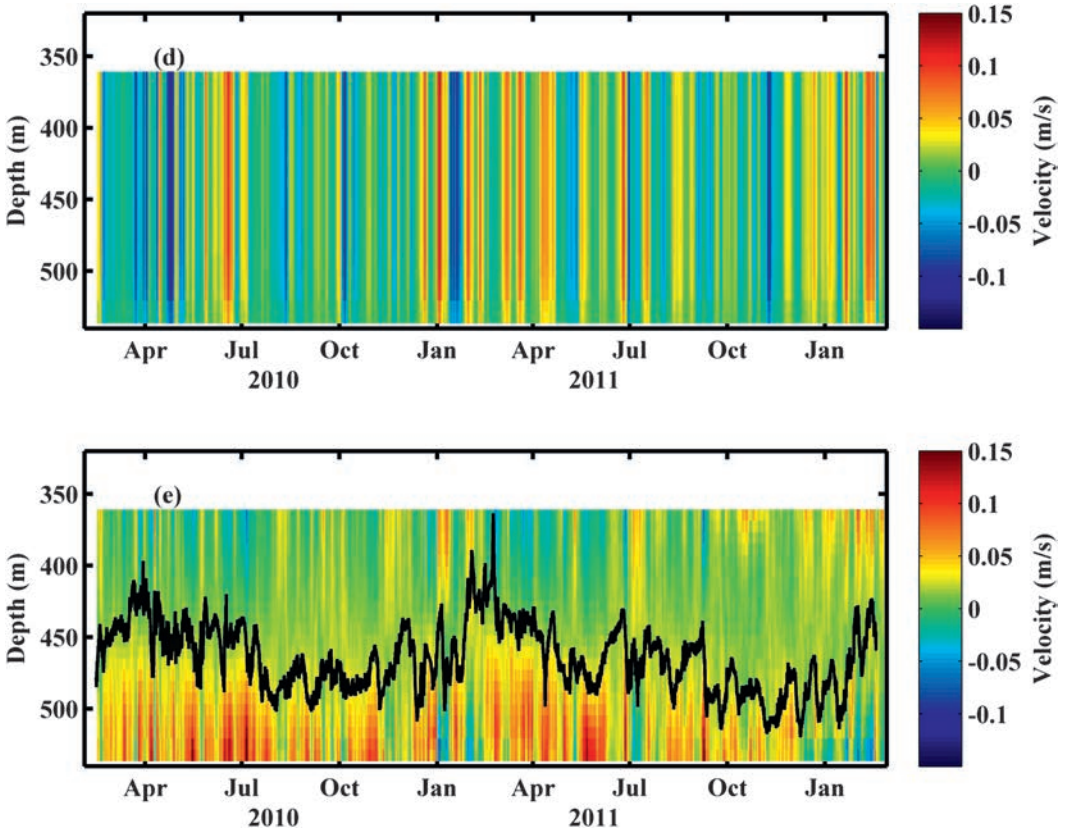

FIG. 5. (*Continued*)

coefficient between bottom temperature and EOF2 has been calculated based on daily ($R = 0.38$), weekly ($R = 0.48$), and monthly ($R = 0.71$) averages, and these were found to be statistically significant [using 99% confidence interval and the large-lag correlation method outlined in Sciremammano (1979)]. The correlation between EOF1 and bottom temperature was not statistically significant for any of these time scales. The fact that the variance of the bottom-intensified flow correlates with bottom temperature indicates that it can be baroclinically forced. The depth-independent EOF1 does not correlate with temperature, which it would have if there were a fluctuating barotropic current moving warm water onto the shelf and cold water off the shelf creating a net heat transport toward the coast. Along-trough sections from the shelf break to the inner shelf have shown previously that isopycnals follow the downhill sloping bathymetry (Jacobs et al. 2011, 2012; Yuan et al. 2013, manuscript submitted to *J. Geophys. Res.*), supporting the idea that the bottom-intensified flow is density driven.

a. Heat fluxes

Equation (1) was integrated forward in time, using the freezing temperature T_F at the observed salinity and pressure as reference temperature, to give a progressive vector plot of the heat flux (Fig. 7a). As can be seen, the dominating heat flux is in the bottom layer and directed along the trough. Estimates of the heat transport were obtained by assuming that $T_R = T_F$ in Eq. (2) and multiplying with the effective width of the channel 80 km [an estimate based on the cross-trough CTD sections in Wåhlin et al. (2010) and Arneborg et al. (2012)]. The parts induced by the total velocity, EOF1, and the residue current (i.e., the total velocity minus EOF1) are shown in Fig. 7. The result is similar to that from the first year of data (Arneborg et al. 2012). EOF1 causes large fluctuations in the daily heat transport (Fig. 7c) for which it accounts for 89% of the variability; however, it does not contribute to the temporal average (Fig. 7b). This is to be expected since EOF1 represents the time-varying part of the barotropic flow and has zero mean. That EOF1 does not contribute to the average heat flow is therefore a direct consequence of the lack of correlation between this mode and the temperature, described above. The residue is comparatively steady and gives the dominant contribution to the temporal average. Also shown (Fig. 7d) is the monthly averages of the heat transport. The monthly averages have smaller

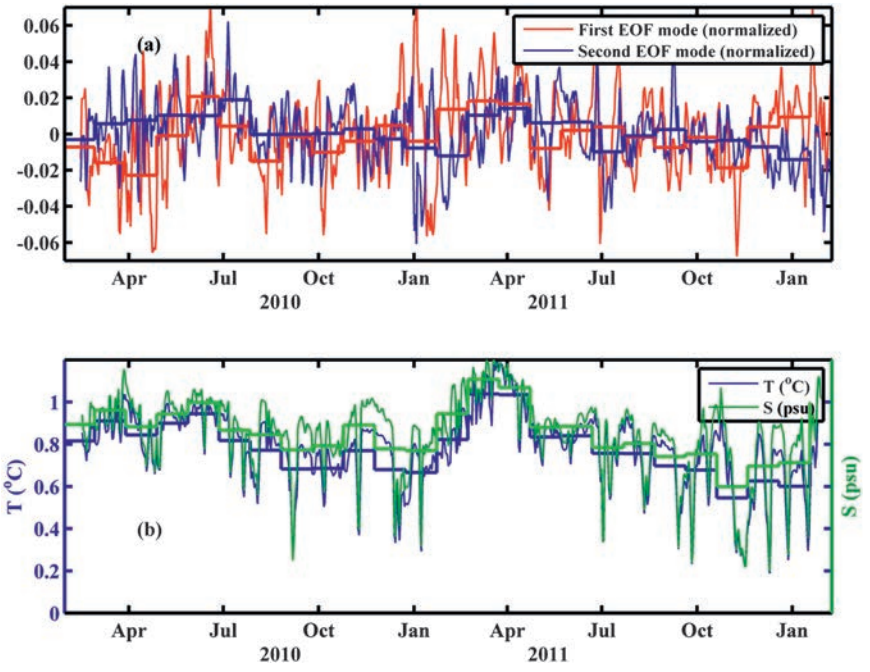

FIG. 6. (a) Time series of first and second EOF modes for the along-trough velocity U. Thin lines indicate daily averages, thick lines indicate monthly averages. (b) Time series of bottom temperature and salinity. Thin lines indicate daily averages, thick lines indicate monthly averages.

variability than the daily averages, and nearly all of this variability is caused by EOF1. Although the monthly averages of total heat transport are always positive (i.e., toward the ice shelves), the part induced by EOF1 is positive in some periods and negative in others.

The integrated heat transport through the deep troughs has previously been estimated based on snapshots of the cross-trough sections (Wåhlin et al. 2010; Walker et al. 2007). Since no time series were available, these studies were forced to assume that only water found off shelf, that is, water denser than neutral density (Jackett and McDougall 1997) $\gamma_N > 28.03$, contributed to the long-term mean. With the present dataset, we are now in a position to arrive at a temporal average using the actual recorded velocity and temperature. During the two years it integrates to 3.4 TW, using Eq. (2), the assumption of an effective width of 80 km, and that $T_R = T_F$. This number is likely an overestimate in relation to the heat available for melting the glacial ice. It was noted in Wåhlin et al. (2010) that water as warm as 0°C shows a meltwater signature, suggesting that at least some of the water only cools to about 0°C before it loses contact with the ice shelves, in which case the reference temperature should be higher than T_F. Using 0°C as reference temperature in Eq. (2) (and integrating only over depths with water warmer than 0°C) gives a significantly lower estimate of 0.95 TW. The mooring data show that the maximum bottom temperature 1.1°C recorded in 2008 (Wåhlin et al. 2010) was unusually warm, and the heat transport estimated in that paper (1.2 TW, from a cross-trough section) is likely larger than the long-term average.

b. Origin of water found on the shelf

Figure 8 shows TS plots of CTD stations occupied during the *Oden* and *Araon* cruises 2008–12 as well as historical data from the National Oceanographic Data Center (NODC) database (Boyer et al. 2006). Figure 8a shows stations on the shelf (red) compared to the off shelf stations (green). Water on the shelf warmer than 0°C aligns on the black-dashed ''Gade line'' (Gade 1979) representing the relationship between T and S for a mixture between warm water and meltwater from glacier ice (Gade 1979; Jenkins and Jacobs 2008).

Figure 8b shows historical off shelf data together with *Oden–Araon* data color coded by depth, and Fig. 8c shows historical off shelf data together with the mooring data. The off shelf water has a distinct temperature maximum at a few hundred meters depth, which is typical for Circumpolar Deep Water (CDW; see e.g., Moffat et al. 2009). Water colder than 1.5°C can be found in two different depth intervals outside the shelf, separated vertically by at least 200 m. For example, water with temperature 1.2°C can be found at about 300-m depth, where it has salinity about 34.57 psu, and

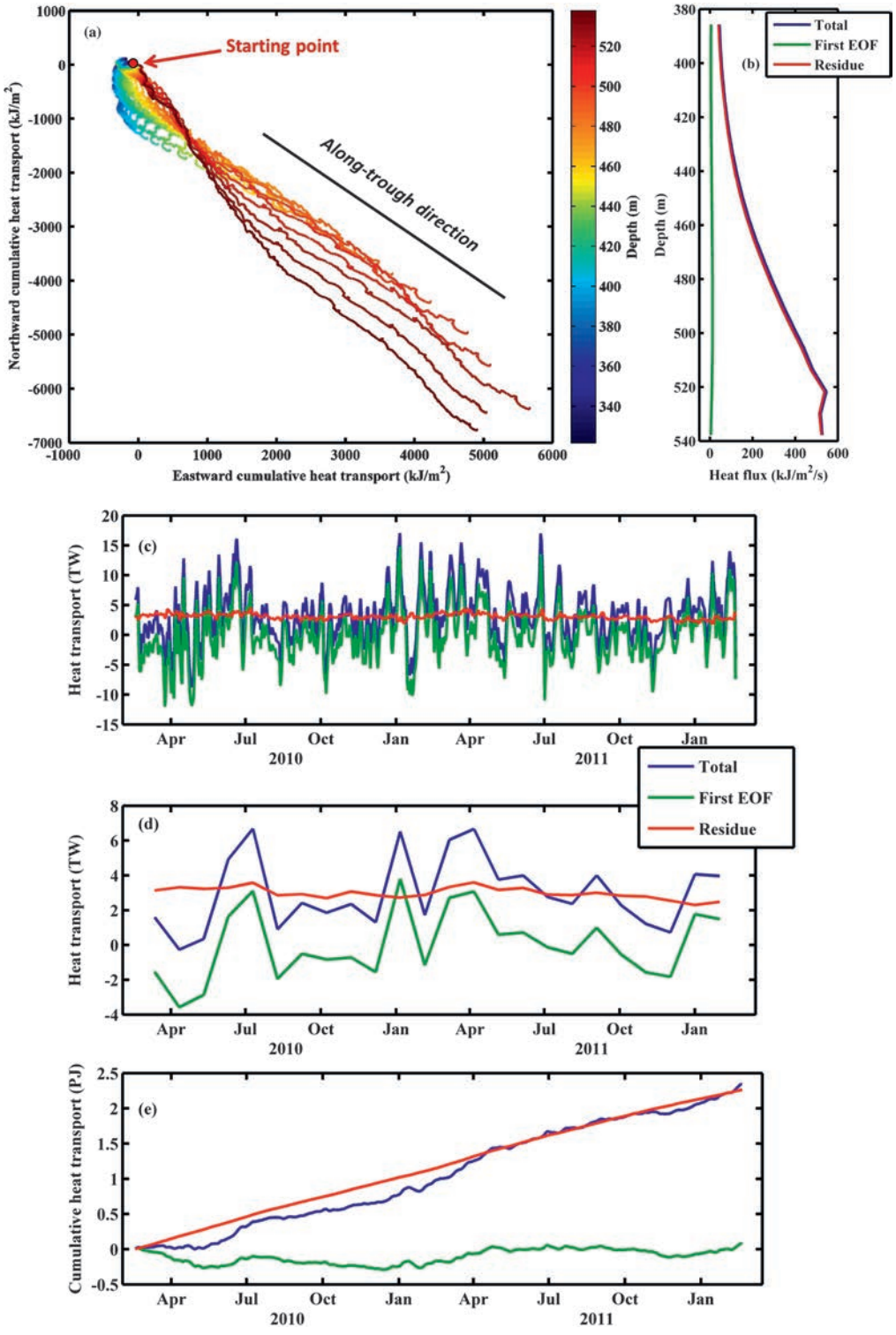

FIG. 7. Heat transport derived from the mooring temperature and velocity. (a) Cumulative heat flux vector according to Eq. (1). (b) Average heat flux due to the total along-trough velocity, the first EOF mode, and the residue (i.e., velocity minus the first EOF mode) according to legend. (c) Daily values of total heat transport as a function of time for the same components as in (b); (d) monthly values of total heat transport as a function of time for the same components as in (b); and (e) cumulative heat transported toward the ice shelves as a function of time for the same components as in (b).

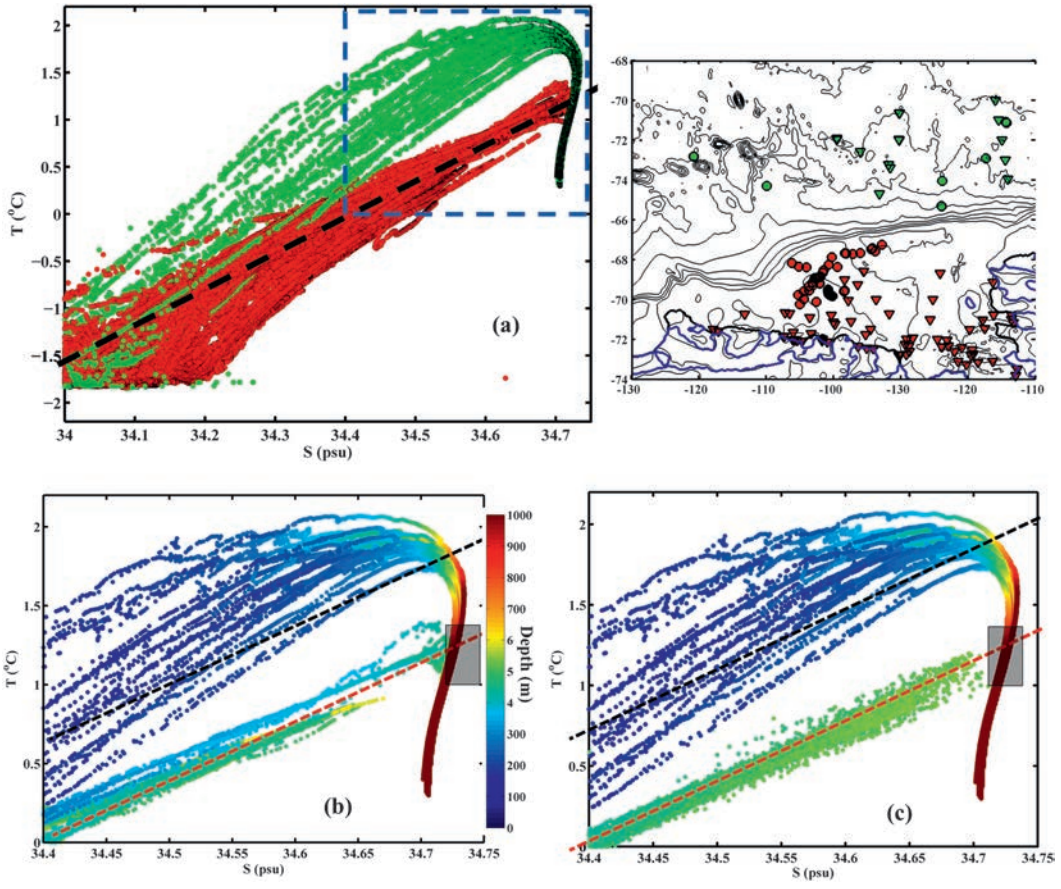

FIG. 8. The *T*–*S* diagram for (a) onshelf data (red) and off shelf data (green) from the four *Oden* and *Araon* cruises during 2008–12 and historical data from the NODC database. Positions of CTD stations are shown in the upper-right panel with dots indicating the *Oden* and *Araon* cruises during 2008–12 and triangles indicating historical data. (b) Historical off shelf data together with *Oden–Araon* data color coded by depth and (c) historical off shelf data together with mooring data color coded by depth. Dashed lines indicate mixing between glacier meltwater and upper CDW (black) and lower CDW (red), shaded rectangle indicates approximate *T*–*S* properties for the unmodified off shelf water, derived by extrapolating the observed meltwater mixing lines on the shelf to the observed the off shelf water *T* and *S*.

also at about 1000-m depth, where it has salinity about 34.71 psu. Using the salinity, it is possible to determine whether the shelf water originated above (upper CDW) or below (lower CDW) the temperature maximum, which has consequences for how we assess the forcing mechanisms. Both the upper and the lower water types can be modified by subsurface melting processes, in which case the modified water products should align on their respective Gade lines (indicated by dashed red and black lines, Fig. 8). Since the on shelf water in the *T*–*S* diagrams falls well below the blue line there is no upper CDW, or meltwater mixtures thereof, in any of the data collected on the shelf.

A noteworthy difference between the Amundsen shelf and Marguerite Trough is the complete lack of upper CDW on the Amundsen shelf, while it is frequently observed on the outer shelf in the Marguerite Trough (Klinck et al. 2004; Moffat et al. 2009; Martinson and McKee 2012). Instead, the water found on the Amundsen shelf appears to be a mixture between glacier meltwater and source water with temperature and salinity bounded by the gray shaded square in Figs. 8b and 8c, that is, source water found below the temperature maximum outside the shelf. The deepest shelf water, found at 500–600 m, comes from depths of at least 1000 m off the shelf. This indicates that some physical mechanisms force the deep water up onto the shelf. Processes that could cause such an uphill movement of the deep water include upwelling induced by along-shelf wind (T08; S12), and an upslope benthic Ekman transport (Wåhlin et al. 2012) induced by eastward currents at the shelf break. We will now proceed to

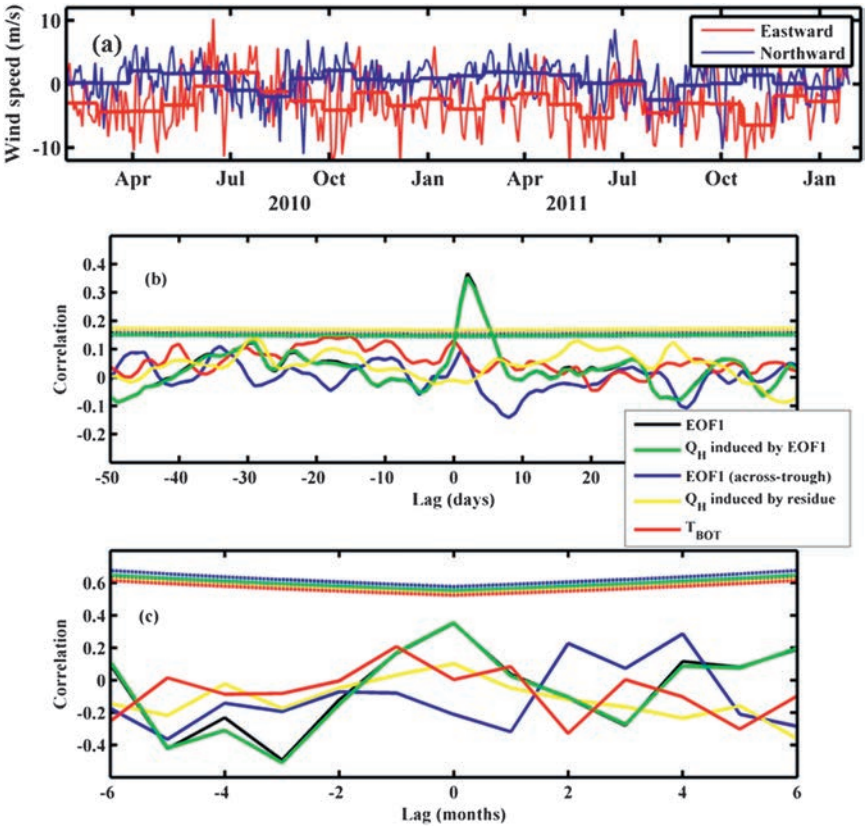

FIG. 9. (a) Daily (thin lines) and monthly (thick lines) values of 10-m wind, averaged over the area indicated by the white rectangle in Fig. 1. Correlation–lag plot between (b) daily and (c) monthly average eastward pseudostress and mooring parameters. Solid lines indicate correlation; dashed lines indicate significance level (Sciremammano 1979), using 99% confidence interval. The investigated parameters are the first EOF mode in the along-trough direction (EOF1), the first EOF mode in the across-trough direction, maximum temperature, heat transport Q_H induced by EOF1 and heat transport Q_H induced by the residue velocity, according to legend.

examine the effect of wind forcing on the flow in the channel. A quantitative examination of the effect of deep shelfbreak currents is not yet possible because of the lack of data from this region but is an important goal for future studies.

4. Wind correlation

Daily and monthly averages of wind, current, and temperature were used to examine the correlation between the mooring data and the wind. Figure 9 shows daily and monthly averages of the eastward wind component from the ERA-Interim data (averaged over the area indicated by the white square in Fig. 1). There is no pronounced seasonal variation in the wind, as noted in the temperature and salinity at the mooring location (Fig. 3), and there is no wintertime maximum as was the case with the National Centers for Environmental Prediction (NCEP) wind during 1990–2004 (T08). Figures 9b and 9c show correlation–lag plots between the eastward pseudostress (i.e., the product of the wind speed and the wind vector), averaged over the white square in Fig. 1, and (black) the EOF1 of along-trough velocity, (blue) the EOF1 of across-trough velocity, (red) bottom temperature, and (green and yellow) the two components of the heat transport caused by the EOF1 and the residue flow (see Fig. 7). For daily values (Fig. 9b), there is a statistically significant correlation between eastward pseudostress and both the EOF1 of along-trough velocity and the heat transport caused by the EOF1 (black and green lines). The maximum correlation is obtained for a time lag of 2.0 days, comparable to the model studies by Dinniman et al. (2011), in which along-shelf wind at the Marguerite Bay correlated positively with flux of warm deep water at a lag of 2.5 days. The obtained correlation indicates that the energetic, short

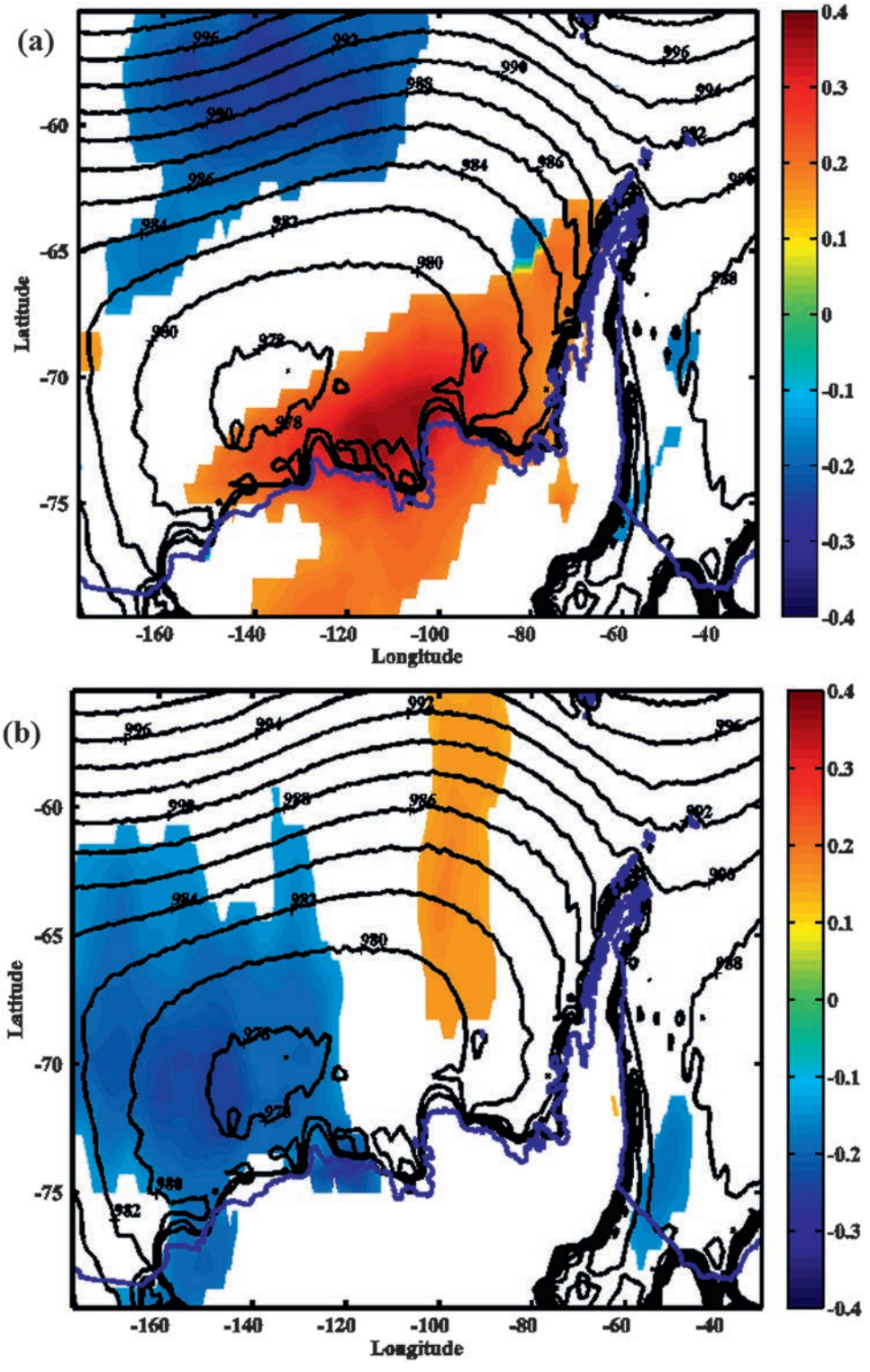

FIG. 10. (a) Correlation between eastward pseudostress at different locations and the first EOF mode in the along-channel direction. Values are according to color bar; white spaces indicate that the correlation was not statistically significant. Black lines show average surface pressure (hPa) during 2010 and 2011. (b) As in (a), but for northward pseudostress. (c) Surface pressure (hPa) averaged over 2010 and 2011 for summer (December–February); fall (March–May), winter (June–August), and spring (September–November).

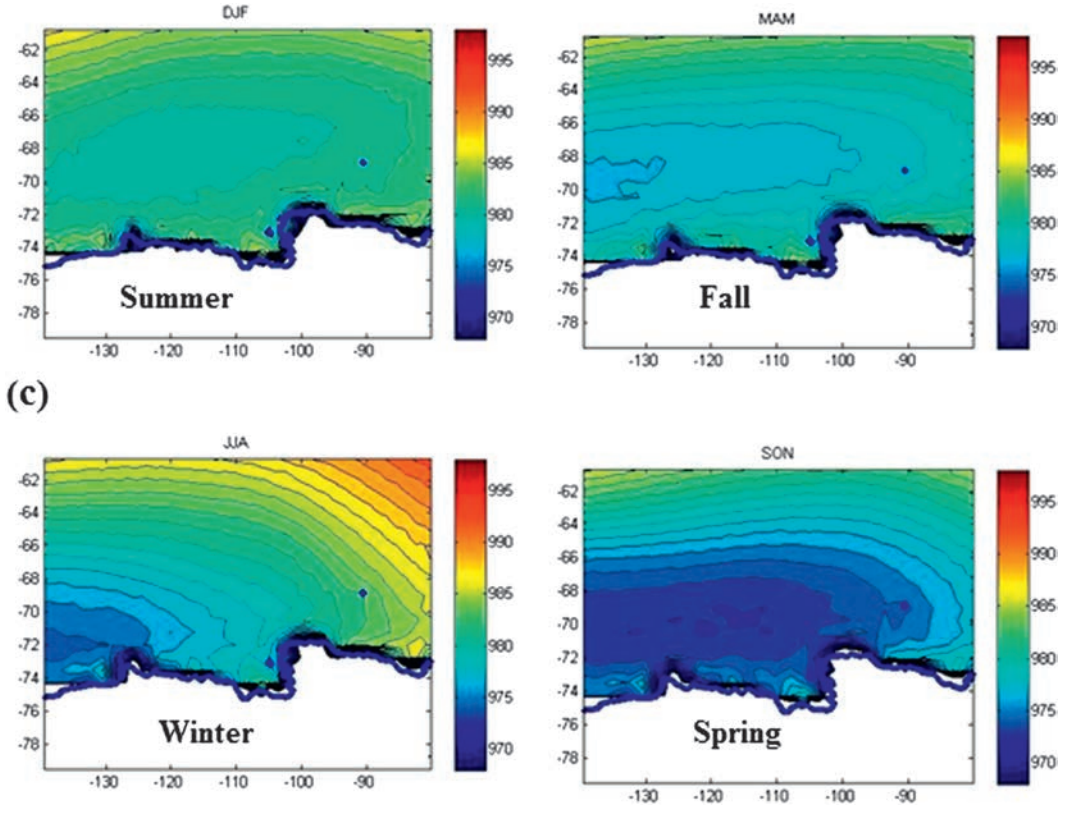

FIG. 10. (*Continued*)

time-scale fluctuations in EOF1 are driven by the wind. The sign of the correlation agrees with standard wind-driven upwelling: eastward winds force an Ekman transport away from the coast, which is compensated by a return flow toward the coast in the deeper water. However, neither the maximum temperature nor the heat transport induced by the residue current is correlated with the wind. This is not surprising since these parameters do not have the energetic daily fluctuations present in EOF1. For the monthly averages (Fig. 9b), none of the examined parameters shows a statistically significant correlation with the along-shelf pseudostress. This means that the seasonal variation of the heat transport evident in Figs. 7d and 7e cannot be shown to be caused by the wind with the present dataset. To examine the correlation on seasonal or longer time scales it is however necessary to have a longer time series.

To examine the spatial variation, maps were constructed showing the strongest significant correlation (at 99% confidence interval) between daily pseudostress at different locations and EOF1 of the along-trough velocity (Figs. 10a,b). White areas indicate that the correlation was not statistically significant. The strongest signal is a positive correlation between EOF1 and eastward wind on the shelf and shelf break (Fig. 10a), but there are areas of significant correlation also with northward wind (Fig. 10b) and an area of negative correlation north of the shelf (Fig. 10a). This reflects the fact that zonal winds at the shelf break are associated with the clockwise circulation in the Amundsen low (T08), visible in the isobars on the maps. Westward winds at the shelf break frequently occur simultaneously with eastward winds at 60°S, northward winds at 130°W, and southward winds at 100°W. No significant correlations were found between the wind and any of the variables bottom temperature, warm-layer thickness, EOF2, and heat transport induced by the residue current.

It can be pointed out that we observe a strong inflow of warm deep water also in the absence of eastward winds. For example, in March–April 2011 there was a 150-m-thick inflow with maximum temperature 1.2°C (Fig. 3), that is, nearly unmodified lower CDW. This inflow was preceded by westward rather than eastward winds (red shaded period in Fig. 2c). A similar maximum in March 2010 was preceded by highly fluctuating winds (red-shaded period in Fig. 2b). In December 2008, a strong inflow of 1.1°C water was recorded along a transect across the channel (Wåhlin et al. 2010), and this was preceded by weak winds that shifted between westward and eastward (red shaded period in Fig. 2a). An inflow

that was weaker than average but occupied the whole width of the channel was recorded in December 2010 (Arneborg et al. 2012), and this was preceded by weak westward winds (Fig. 2b). Figure 10c shows the surface pressure averaged over the seasons. The southward migration of the Amundsen low that is expected in wintertime (e.g., T08) was nearly absent during 2010 and 2011 (cf., e.g., Fig. 10c to Fig. 4 in T08), and as a consequence the winds at the shelf break were westward rather than eastward (Fig. 9a). It is possible that strong, prevailing eastward winds at the shelf break, absent during the present measurement period, would change the correlation results obtained here.

5. Discussion

A 2-yr time series of the flow of warm deep water in one of the deep troughs on the Amundsen shelf has here been presented for the first time. During these two years there was a constant presence of warm water with monthly average above 0.6°C in the trough but also a marked seasonal variation with warm-layer thickness and bottom temperature peaking in late summer and early fall. Observations from the inner shelf near the Dotson glacier during a 10-month period in 2006 (Jacobs et al. 2012) show a similar degree of variability in temperature, but cooler water (0.3°–0.8°C) and no pronounced maximum in March–May. This discrepancy could be due to the fact that the 2006 mooring was located in the center of one of the deep basins, where mechanisms such as internal waves and basin-scale eddies can affect the time variability. This fits well with the model results of Schodlok et al. (2012) who find no direct coupling between the inner and outer shelf dynamics.

The velocity below 360-m depth as covered by the observations is characterized by energetic fluctuations, nearly barotropic in nature, and a more slowly varying inflow of warm water next to the bottom (Fig. 5). A qualitative examination of the barotropic fluctuations shows that eastward (westward) wind along the shelf break sets up a southeastward (northwestward) velocity in the along-trough direction, as expected from wind-driven Ekman upwelling (downwelling). The time lag for the maximum correlation between along-shelf winds and along-trough flow is 2 days (Fig. 9b), similar to model results from Marguerite Trough (Dinniman et al. 2011). Unlike in the Marguerite Trough, however, there is no middepth warm water (upper CDW) advected across the shelf with the barotropic flow (Klinck et al. 2004; Dinniman and Klinck 2004; Moffat et al. 2009; Martinson and McKee 2012). The fact that there are no historical observations of upper CDW on the Amundsen shelf (Fig. 7) indicates that the wider continental shelf effectively blocks the ice shelves from contact with this water mass. The effect of wind on the transport of oceanic heat to the ice shelves is thus likely fundamentally different in the two shelf regions. Process-oriented experiments with an eddy-resolving ocean model (St. Laurent et al. 2013) identified topographic interactions with the shelfbreak currents as a key mechanism for creating on-shore flow of warm water in the troughs. Further model studies capturing these dynamics would be useful.

The present results together with previous studies indicate that the near-bottom flow is forced by gravity as the relatively dense warm water descends from the shelf break to greater depths in the inner shelf basins. However, the water that enters at the shelf break originates from depths greater than the trough sill outside the shelf (Fig. 8). It is easy to be misled by only looking at temperature sections, to assume that the water that crosses the shelf break originates from above the temperature max and flows from 200–300-m depth outside the shelf all the way to the inner shelf basins. The water in the eastern inner shelf basin has temperature 1°–1.2°C (e.g., Jacobs et al. 2012; Yuan et al. 2013, manuscript submitted to *J. Geophys. Res.*) and salinity of about 34.7 psu (e.g., Yuan et al. 2013, manuscript submitted to *J. Geophys. Res.*; Wåhlin et al. 2012). The warm water on the shelf can hence be traced to depths below 500 m outside the shelf. A physical mechanism is needed to force the deep water up the slopes before it can flow down into the inner shelf basins aided by gravity. It was shown in Wåhlin et al. (2012) that water is at least occasionally forced along the bottom up from 1000- to 1200-m depth onto the top of the shelf break. This can also be seen in the outer part of section (b) in Jacobs et al. (2012).

One possible forcing mechanism for upslope flow is wind-driven upwelling. The results presented here show, however, that the wind is not of primary importance for the warm-layer thickness or temperature in this region. The wind does, however, give rise to energetic short-term variability in the whole sampled water column. This is evident because of a strong positive correlation between daily eastward wind and EOF1—the most energetic mode, which is nearly depth independent. On longer time scales the correlation disappears and the monthly averages of wind and EOF1 have nonsignificant correlation. However, the present dataset is rather short for quantitative studies of seasonal variation. It could well be that a significant correlation would be found with a longer dataset—with 4 yr of data the significance level is reduced to about 0.3 provided the variance in the time series remains on the same level.

The only existing model studies for the Amundsen shelf have a strong focus on the region farther east, in the vicinity of Pine Island Bay (PIB) (T08; S12;

Schodlok et al. 2012). The observational data contradict the model results of T08 and S12 in two aspects. First, the modeled seasonal variation of the warm-layer thickness has a pronounced maximum in September–November (T08; S12). A seasonal variation of bottom temperature is present in the observational data but the maximum occurs in March–May instead. In Schodlok et al. (2012) the heat transport was examined, based on the streamfunction and temperature, and this was found to have seasonal maximum at the same time as the observations. Second, the modeled warm-layer thickness correlates with eastward winds (S12), but no such correlation was found in the data. The positive correlation between the daily wind and the energetic barotropic fluctuations (EOF1) found in the data is expected from wind-driven upwelling theories. This correlation was statistically significant for daily averages. However, for longer time scales (monthly averages) as used in the models (T08; S12) the correlation was not statistically significant. The short-term variability in EOF1 does induce a short-term variability in the heat transport, which also correlates with eastward winds. This component does not give any contribution to the long-term heat transport. There is a variation in the heat transport also on monthly and longer time scales (Fig. 7d), coupled to EOF1, but this variation cannot be said to correlate with the wind. The calculated correlation was not statistically significant. However, it should be stressed that the time series is most likely too short to draw robust conclusions about seasonal variations of velocity or heat transport. It should also be pointed out that the years 2010 and 2011 had wintertime eastward winds that were considerably weaker than average climatology (e.g., T08; S12), and that the model studies T08 and S12 focus on the eastern trough, which may have other forcing mechanisms than the central [as suggested, e.g., in Wåhlin et al. (2012)].

An alternative forcing mechanism other than wind is upslope benthic Ekman transport induced by deep-reaching currents along the continental slope. The phenomenon has been observed in the eastern part of the shelf break (Wåhlin et al. 2012). A recent study suggests that the deep-reaching currents are baroclinically forced and are an inherent feature of the shelf slope current system in the east (Walker et al. 2013), which would indicate that upslope benthic Ekman transport is regularly occurring there. We hypothesize that Ekman pumping is indeed a primary factor forcing lower CDW over the shelf break in the east and into PIB. After interacting with the shelf ice and icebergs in the eastern basin, the then slightly colder and fresher warm water flows northward along the midshelf ridge and follows the topography west and then turns into the central trough. Supporting this hypothesis are recent studies (Yuan et al. 2013, manuscript submitted to *J. Geophys. Res.*; Wåhlin et al. 2012; Jacobs et al. 2012) showing that the deep water is substantially fresher and cooler on the central shelf than on the east, a property that is also seen in the mooring data and the historical data presented here (Fig. 8). While pure lower CDW of temperature 1.1°C and warmer is commonly found in the eastern basin (e.g., Jacobs et al. 2012 and references therein), only the fresher and colder ''Gade water'' derivatives of it can be found in the central shelf region. Water as cold as 0°C has an average velocity toward the ice shelves in the central trough (Fig. 4b), indicating that subsurface modification by icebergs or ice shelves has already taken place when the water enters the central shelf and flows toward the Dotson and Getz ice shelves (see also Yuan et al. 2013, manuscript submitted to *J. Geophys. Res.*). Synoptic measurements from the eastern and western shelf and continental slope are needed to test this hypothesis.

Acknowledgments. Oden Southern Ocean 2009/10 and 2010/11 cruises were supported by the National Science Foundation, Swedish Polar Research Secretariat, and the Swedish Research Council (SRC). Support for mooring construction was Grant KAW2007.0107 from the K&A Wallenberg Foundation and the Swedish Research Council (through Grant 2011-5263). *Araon* cruises (ANA01C and ANA02C) were supported by KOPRI Grants PP12010 and PP13020. AKW, LA, and GB were supported by SRC through Grants 2010-19172-73868-33, 824-2008-6439, and 621-2008-2689. We are indebted to Martin Jakobsson, Chrissie Wiederwohl, and Alex Orsi for making mooring deployment possible in 2010. T. J. Choi kindly provided the wind data collected in Lindsey Island. We are also grateful to the Captains, crews, and technical personnel on board IB *Oden* and IB *Araon* for expert skill and enthusiasm.

REFERENCES

Arneborg, L., A. Wåhlin, G. Björk, B. Liljeblad, and A. Orsi, 2012: Persistent inflow of warm water through a submarine trough on the central Amundsen shelf. *Nat. Geosci.,* **5,** 876–880.

Boyer, T. P., and Coauthors, 2006: *World Ocean Database 2005.* NOAA Atlas NESDIS 60, 190 pp.

Bracegirdle, T. J., and G. J. Marshall, 2012: The reliability of Antarctic tropospheric pressure and temperature in the latest global reanalyses. *J. Climate,* **25,** 7138–7146.

Carvajal, G. K., L. E. B. Eriksson, and L. M. H. Ulander, 2013: Retrieval and quality assessment of wind velocity vectors on the ocean with C-band SAR. *IEEE Trans. Geosci. Remote Sens.,* **99,** 1–19.

Davis, R. E., 1976: Predictability of sea surface temperature and sea level pressure anomalies over the North Pacific Ocean. *J. Phys. Oceanogr.,* **6,** 249–266.

Dee, D. P., and Coauthors, 2011: The ERA-Interim reanalysis: Configuration and performance of the data assimilation system. *Quart. J. Roy. Meteor. Soc.,* **137,** 553–597, doi:10.1002/qj.828.

Dinniman, M. S., and J. M. Klinck, 2004: A model study of circulation and cross-shelf exchange on the west Antarctic Peninsula continental shelf. *Deep-Sea Res. II,* **51,** 2003–2022.

——, ——, and W. Smith, 2011: A model study of Circumpolar Deep Water on the West Antarctic Peninsula and Ross Sea continental shelves. *Deep-Sea Res. II,* **58,** 1508–1523.

Gade, H., 1979: Melting of ice in sea water: A primitive model with application to the Antarctic ice shelf and icebergs. *J. Phys. Oceanogr.,* **9,** 189–198.

Jackett, D. R., and T. R. McDougall, 1997: A neutral density variable for the world's oceans. *J. Phys. Oceanogr.,* **27,** 237–263.

Jacobs, S., A. Jenkins, C. Giulivi, and P. Dutrieux, 2011: Stronger ocean circulation and increased melting under Pine Island Glacier ice shelf. *Nat. Geosci.,* **4,** 519–523, doi:10.1038/NGEO1188.

——, ——, H. Hellmer, C. Giulivi, F. Nitsche, B. Huber, and R. Guerrero, 2012: The Amundsen Sea and the Antarctic Ice Sheet. *Oceanography,* **25,** 154–163, doi:10.5670/oceanog.2012.90.

Jenkins, A., and S. Jacobs, 2008: Circulation and melting beneath George VI ice shelf, Antarctica. *J. Geophys. Res.,* **113,** C04013, doi:10.1029/2007JC004449.

Klinck, J. M., E. E. Hofmann, R. C. Beardsley, B. Salihoglu, and S. Howard, 2004: Water-mass properties and circulation on the west Antarctic Peninsula continental shelf in austral fall and winter 2001. *Deep-Sea Res. II,* **51,** 1925–1946, doi:10.1016/j.dsr2.2004.08.001.

Lee, S. H., and Coauthors, 2012: The Amundsen Sea Expedition 2012 (ANA02C), cruise report. KOPRI Rep., 138 pp.

Martinson, D. G., and McKee, D. C., 2012: Transport of warm Upper Circumpolar Deep Water onto the western Antarctic Peninsula continental shelf. *Ocean Sci.,* **8,** 433–442, doi:10.5194/os-8-433-2012.

Moffat, C., B. Owens, and R. C. Beardsley, 2009: On the characteristics of Circumpolar Deep Water intrusions to the west Antarctic Peninsula continental shelf. *J. Geophys. Res.,* **114,** C05017, doi:10.1029/2008JC004955.

Pawlowicz, R., B. Beardsley, and S. Lentz, 2002: Classical tidal harmonic analysis including error estimates in MATLAB using T_TIDE. *Comput. Geosci.,* **28,** 929–937.

Pritchard, H. D., R. J. Arthern, D. G. Vaughan, and L. A. Edwards, 2009: Extensive dynamic thinning on the margins of the Greenland and Antarctic ice sheets. *Nature,* **461,** 971–975.

——, S. Ligtenberg, H. Fricker, D. Vaughan, M. van der Broeke, and L. Padman, 2012: Antarctic ice-sheet loss driven by basal melting of ice shelves. *Nature,* **484,** 502–505, doi:10.1038/nature10968.

Schodlok, M., D. Menemenlis, E. Rignot, and M. Studinger, 2012: Sensitivity of the ice-shelf/ocean system to the sub-ice-shelf cavity shape measured by NASA IceBridge in Pine Island Glacier, West Antarctica. *Ann. Glaciol.,* **53,** 156–162, doi:10.3189/2012AoG60A073.

Sciremammano, F., Jr., 1979: A suggestion for the presentation of correlations and their significance levels. *J. Phys. Oceanogr.,* **9,** 1273–1276.

Shepherd, A., D. Wingham, J. Mansley, and H. Corr, 2001: Inland thinning of Pine Island Glacier, West Antarctica. *Science,* **291,** 862–864, doi:10.1126/science.291.5505.862.

——, ——, and E. Rignot, 2004: Warm ocean is eroding West Antarctic Ice Sheet. *Geophys. Res. Lett.,* **31,** L23402, doi:10.1029/2004GL021106.

Steig, E., Q. Ding, D. S. Battisti, and A. Jenkins, 2012: Tropical forcing of Circumpolar Deep Water inflow and outlet glacier thinning in the Amundsen Sea Embayment, West Antarctica. *Ann. Glaciol.,* **53,** doi:10.3189/2012AoG60A110.

St. Laurent, P., J. Klinck, and M. Dinniman, 2013: On the role of coastal troughs in the circulation of warm Circumpolar Deep Water on Antarctic Shelves. *J. Phys. Oceanogr.,* **43,** 51–64.

Thoma, M., A. Jenkins, D. Holland, and S. Jacobs, 2008: Modelling Circumpolar Deep Water intrusions on the Amundsen Sea continental shelf, Antarctica. *Geophys. Res. Lett.,* **35,** L18602, doi:10.1029/2008GL034939.

Wåhlin, A. K., X. Yuan, C. Nohr, and G. Björk, 2010: Inflow of warm Circumpolar Deep Water in the Western Amundsen Sea. *J. Phys. Oceanogr.,* **40,** 1427–1434.

——, R. D. Muench, L. Arneborg, G. Björk, H. K. Ha, S. H. Lee, H. Alsén, 2012: Some implications of Ekman layer dynamics for cross-shelf exchange in the Amundsen Sea. *J. Phys. Oceanogr.,* **42,** 1461–1474.

Walker, D. P., M. A. Brandon, A. Jenkins, J. T. Allen, J. A. Dowdeswell, and J. Evans, 2007: Oceanic heat transport onto the Amundsen Sea shelf through a submarine glacial trough. *Geophys. Res. Lett.,* **34,** L02602, doi:10.1029/2006GL028154.

——, A. Jenkins, K. M. Assmann, D. R. Shoosmith, and M. A. Brandon, 2013. Oceanographic observations at the shelf break of the Amundsen Sea, Antarctica. *J. Geophys. Res. Oceans,* **118,** 2906–2918, doi:10.1002/jgrc.20212.